JOURNAL OF GEOPHYSICAL RESEARCH, VOL. 95, NO. C2, PAGES 1681–1691, FEBRUARY 15, 1990

On the Sensitivity of Sverdrup Transport Estimates to the Specification of Wind Stress Forcing in the Tropical Pacific

MARY C. LANDSTEINER

School of Oceanography, University of Washington, Seattle

MICHAEL J. MCPHADEN

NOAA Pacific Marine Environmental Laboratory, Seattle, Washington
School of Oceanography, University of Washington, Seattle

JOËL PICAUT

Groupe SURTROPAC, Institut Francais de Recherche Scientifique Pour le Développement en Coopération (ORSTOM), Nouméa, New Caledonia

We use Sverdrup dynamics to estimate geostrophic transports between 20°N and 20°S in the tropical Pacific Ocean averaged over the period 1979–1981. Three wind stress products are used to force the model. Results are compared to geostrophic transports computed along expendable bathythermograph transects in the western, central, and eastern Pacific for the same period. Depending on the choice of wind stress, modeled transports may differ from the observations by a factor of 2 and, in some cases, flow is opposite to that observed. Possible limitations of the Sverdrup theory are discussed; however, we conclude that detailed and accurate simulation of the general circulation in the tropical Pacific is limited more by the uncertainties in presently available estimates of the surface wind stresses than by deviations from Sverdrup balance.

1. INTRODUCTION

Occurrences of El Niño (EN) and swings in the Southern Oscillation (SO) have been related to instabilities of the coupled ocean-atmosphere system [*Zebiak and Cane*, 1987; *Schopf and Suarez*, 1988]. Since ENSO events may be predictable [e.g., *Cane et al.*, 1986], efforts are underway to develop an operational ocean-atmosphere model for climate prediction as part of the Tropical Ocean–Global Atmosphere (TOGA) program. In the tropics, coupling on climatic time and space scales is through sea surface temperature (SST) variations (which drive the atmosphere) and wind stress variations (which drive the ocean). Wind-driven ocean circulation is a crucial determinant in SST variability, so an intermediate step in the development of an operational coupled model has been to test the sensitivity of ocean model simulations to prescribed wind stress forcing.

Recent tropical Pacific Ocean model simulations have been useful in quantifying the errors that can be expected in modeled variability due to imprecisely known surface wind stresses. *McPhaden et al.* [1988] found in a series of linear, multi-vertical mode model simulations, using three different wind stress products, that typically only 25–50% of the variance in the observed sea level and surface dynamic height could be modeled at the annual period. Moreover, the coherence between simulations themselves was only 0.6–0.8, suggesting that 1/3 to 2/3 of the modeled variance depends on the particular choice of wind stress product. In a series of simulations using a general circulation model driven by five different wind stress products, *Harrison et al.* [1989] found that dynamic height and subsurface temperature anomalies associated with the 1982–1983 El Niño were reasonably well hindcast within several degrees of the equator. However, at higher latitudes in the tropics the differences between simulated and observed variations were often comparable to, or larger than, observed variations. Furthermore, SST anomalies were not well modeled at any latitude.

In this study, we address a simpler question than that of *McPhaden et al.* [1988] or *Harrison et al.* [1989], namely, how sensitive are simulations of the mean circulation in the tropical Pacific to the specification of surface wind stress? We use *Sverdrup*'s [1947] model for linear, steady state, depth-integrated flow away from western boundaries. It is assumed that this model is relevant to the tropical Pacific as was found for the North Atlantic Ocean [*Leetmaa et al.*, 1977], where possible limitations to Sverdrup theory will be discussed in a later section. Although error characteristics of the wind fields used in this study are not well defined, the effects of random errors on the simulations should be minimized because of the time and zonal averaging inherent in Sverdrup dynamics. Thus it is possible that simulations of the long-term mean may be less sensitive to the specification of wind stress than the simulations of annual and interannual variations.

Previous calculations of basin-wide Sverdrup circulation in the tropical Pacific include those of *Welander* [1959], *Evenson and Veronis* [1975], *Meyers* [1980], *Kessler and Taft* [1987], *McPhaden and Fine* [1988], and *Godfrey* [1989]. Our study is distinguished from these in that we obtain solutions for three different wind products for the period 1979–1981; the longest coincident non–El Niño period for these products at the time of this work. These wind products are the same as used by *McPhaden et al.* [1988], namely, the

Paper number 89JC02792.
0148-0227/90/89JC-02792$05.00

Florida State University (FSU) winds [*Goldenberg and O'Brien*, 1981], the University of Hawaii (UH) winds [*Sadler et al.*, 1987], and the U. S. Navy Fleet Numerical Oceanography Center (FNOC) winds [*Halpern and Harrison*, 1982]. Furthermore, we compare model results to the augmented ship of opportunity (SOP) expendable bathythermograph (XBT) data [*McPhaden et al.*, 1988] collected in the western, central, and eastern Pacific during the same 3-year period. Using the same time period helps to minimize ambiguities in the comparison of model results with observations that might arise on account of nonstationarity in the wind field and ocean on multiyear time scales. However, the XBT data are limited to 400 m depth and require use of a mean temperature-salinity (T-S) relation to calculate dynamic height and geostrophic transport. Hence additional comparisons are made with the historical hydrographic data of *Levitus* [1982].

The remainder of this paper is outlined as follows. In section 2 we present a brief discussion of the wind, XBT, and Levitus data sets. Section 3 reviews Sverdrup dynamics relevant to this study. In section 4, maps of Sverdrup stream function and geostrophic transport per unit width are presented. In section 5 we compare both XBT and Levitus data calculations and XBT and model results along SOP XBT transects. Finally, in section 6 we conclude with a brief summary and discussion.

2. DATA

2.1. *Wind Products*

The wind data were reduced to cover the oceanic area of 21°N to 21°S by 124°E to 70°W on a 2° by 2° grid. For all the wind products, the stresses exerted on the ocean surface are calculated using the square drag law with a constant drag coefficient ($C_d = 1.5 \times 10^{-3}$) and air density ($\rho_a = 1.2$ kg m^{-3}). The uncertainty in the drag coefficient is about 10–20% [*Large and Pond*, 1981], which in our linear model yields uncertainties proportional to the magnitude of the model response.

The FSU wind product is a subjective analysis derived from ship wind reports. Horizontal components of pseudostress (i.e., $|\mathbf{v}|\mathbf{v}$, where $\mathbf{v}$ is wind velocity) are calculated for each individual wind measurement. The pseudostresses are collected in bins of 2° latitude by 10° longitude by 1-month and analyzed using methods described by *Goldenberg and O'Brien* [1981]. They are then contoured and interpolated to a 2° by 2° grid. Ship wind observations are generally more numerous in the northern hemisphere than in the southern and tend to be concentrated along a few major shipping lanes.

The UH analysis is a subjectively analyzed composite of GOES satellite-observed, low-level cloud motion vectors and ship, buoy, and island winds. The cloud motion vectors are calibrated to near-surface wind vectors using a climatological shear between historical cloud motion vectors and ship winds as described in *Sadler and Kilonsky* [1985]. Because of a lack of satellite coverage west of the date line during 1979–1981, data from ships, buoys, and islands were exclusively used in that region. Data are initially grouped in 2.5° latitude by 5° longitude bins for reduction [*Sadler et al.*, 1987] and then contoured, interpolated, and reported as monthly averages on a 2.5° by 2.5° grid. We interpolated the data to the 2° by 2° FSU grid to standardize further computations. In general, UH winds have a better spatial and temporal coverage than FSU winds. However, this is not true in areas generally free of clouds (such as eastern basin coastlines) or in areas of high clouds where low-level clouds are obscured. The latter effect is common in convergence zones where deep convection occurs. Biases in wind speeds of $O(1$ m s$^{-1})$ may result from data gaps in cloud winds during periods of weakening or reversal of easterlies or strengthening of northerlies [*Mitchum*, 1987].

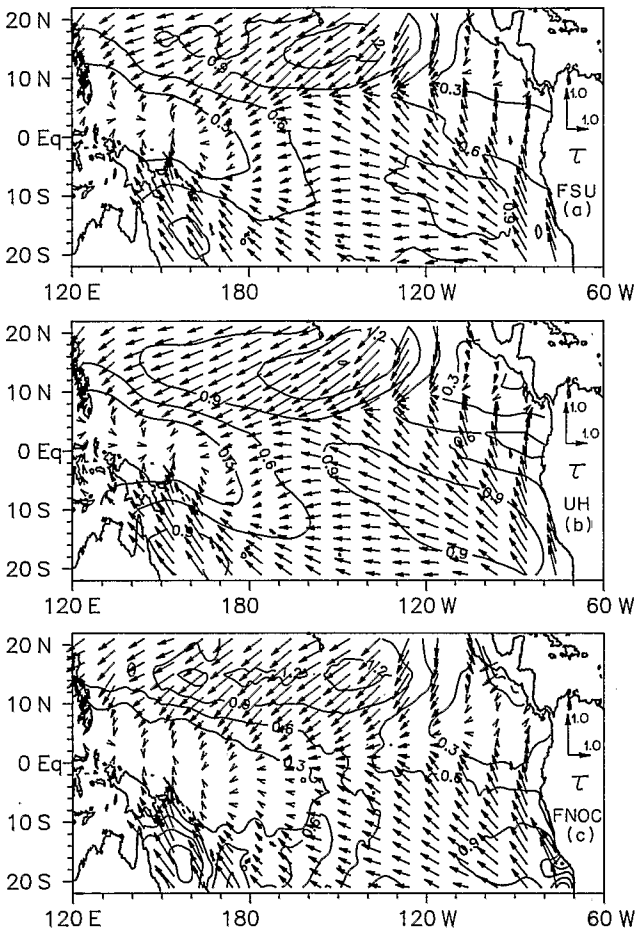

Fig. 1. Vector mean wind stress overplotted on contours of wind stress magnitude (in dynes per square centimeter) for (*a*) FSU, (*b*) UH, and (*c*) FNOC analyses. The unit vector in the meridional direction is stretched to preserve direction relative to geographical coordinates. The contour interval is 0.3 dyn cm^{-2}.

The FNOC operational wind product, generated every 6 hours, is based on a purely objective analysis technique, as described by *Halpern and Harrison* [1982]. This method incorporates measurements from all available sources: island and land stations, ship and buoy winds, low-level cloud vector winds, and winds (and their gradients) inferred from pressure (away from the equator). If no data are available for a given period, previous analysis and climatology are used. Data were initially analyzed on a 2.5° by 2.5° grid, then contoured and interpolated onto a 2° by 2° grid and reported as monthly means.

Monthly values for each wind product were averaged over the period 1979–1981. Vector plots of the 3-year time average mean wind stress, superimposed on contours of the wind stress magnitude, are presented in Figure 1. Plots of the

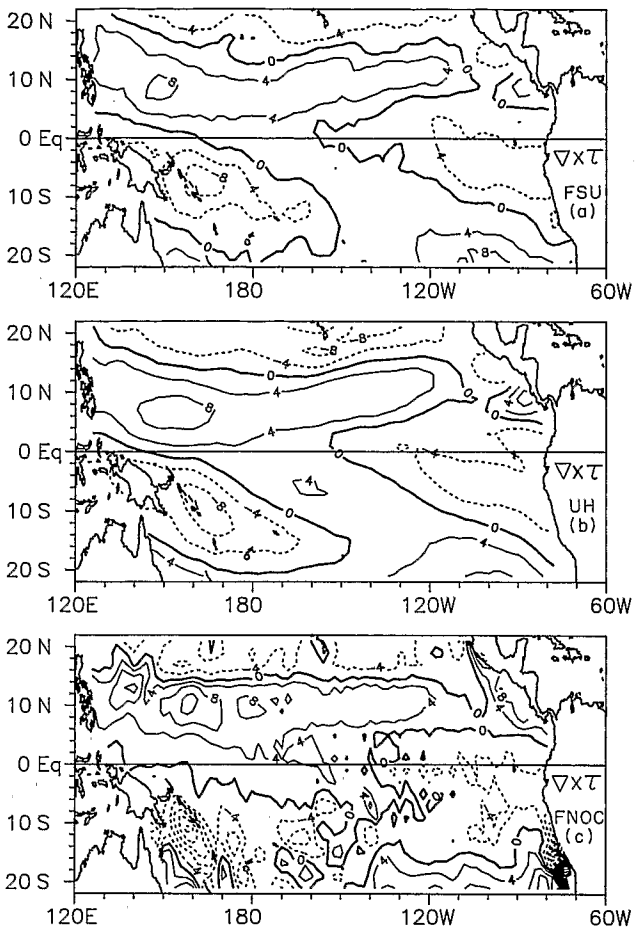

Fig. 2. Mean wind stress curl (in units of 10^{-8} dyn cm^{-3}) for (*a*) FSU, (*b*) UH, and (*c*) FNOC analyses. The contour interval is 4 × 10^{-8} dyn cm^{-3}.

individual zonal and meridional mean stress components for the same period and their standard deviations have been presented by *McPhaden et al.* [1988]. All three wind products depict the general equatorial trade wind system, with UH tending to be smoother and stronger and FNOC having more small-scale variability, especially along coastlines. Additionally, the FNOC product has a few anomalous large-scale features in contrast to the FSU or UH products. In particular, the Intertropical Convergence Zone (ITCZ) in the FNOC product is closer to the equator in the eastern basin, resulting in strong northerlies just north of the equator. Also, in the FNOC product, the southeast trades in the eastern basin are weaker than in both the FSU and UH products, with the core magnitude oriented zonally rather than oriented northwest-southeast.

Plots of the mean curl fields are shown in Figure 2 and can also be found along with plots of their standard deviations in *McPhaden et al.* [1988]. Curls were calculated using a centered, second-order, finite difference scheme. The curl fields are dominated by banded structure, the zeros of which are typically coincident with minima and maxima of the zonal stress. As with the stress fields, the UH curl field is the smoothest and the FNOC curl field has the most small-scale variability. In general, the same large-scale patterns appear in all three products. The most significant qualitative difference is in the southern basin where the FNOC curl shows a noisy but almost unbroken band of negative curl across the basin between about 5° and 15°S, whereas both the FSU and UH negative curl regions in the southern basin are definitely divided by a positive curl band that parallels the South Pacific Convergence Zone SPCZ. Also, the core of the negative curl signal off northeast Australia is shifted further south in the FNOC product than in either the FSU or UH product.

2.2. *Oceanic Data*

Depth-integrated pressures and geostrophic transports were calculated along ship of opportunity transects in the western (20°N, 150°E to 20°S, 165°E), central (20°N, 150°W to 20°S, 180°), and eastern (7°N, 80°W to 20°S, 150°W) Pacific using both augmented XBT data from the period 1979–1981 and *Levitus*' [1982] historical salinity and temperature data. XBT data from the SOP program [*Meyers and Donguy*, 1980] have been augmented with additional independent XBT data, conductivity-temperature-depth (CTD) data, and hydrocast data from the same period; for convenience we will refer to this combined data set as XBT data. The collection and processing of the data is summarized by *McPhaden et al.* [1988]. Data from subjectively determined longitudinal regions [see *McPhaden et al.*, 1988, Figure 1*b*] were grouped in 1° latitudinal bins, then smoothed spatially to eliminate all wave numbers higher than 0.33 cycles per degree of latitude. Dynamic heights relative to 400 m (76% of the XBTs reach this depth) were calculated using along-track mean *T-S* relations determined from the *Levitus* [1982] data set described below. As discussed by *Kessler and Taft* [1987], *McPhaden et al.* [1988], and J. Picaut and R. Tournier (manuscript in preparation, 1989), at least a ±2 dyn cm error in calculations of monthly mean dynamic heights can be expected due to data sampling, grouping into transects, and use of a mean *T-S* relationship. This error will be reduced for the 3-year averages to the extent that it is in part random, possibly to ±1 dyn cm assuming a decorrelation time scale for upper ocean temperature of 6 months [*White et al.*, 1982].

The *Levitus* [1982] data set is on a 1° by 1° horizontal grid at discrete depths from the surface to the ocean bottom (maximum depth of 5500 m). It is a composite of all historical data from the oceanographic station data (CTD and STD (salinity-temperature-depth) casts from 1900–1978), XBTs (1966–1977), and mechanical bathythermographs (MBTs) (1941–1977), which has been objectively analyzed at each depth using a successive corrections method similar to that of *Cressman* [1959]. The effective resolution of the data depends on data density, since the gridding technique fills in data-sparse regions with large-scale information but retains some smaller-scale information where data are plentiful. Resolution may therefore be better in the northern hemisphere than in the southern where data coverage was more sparse. However, there is always significant smoothing due to the analysis procedure which uses, minimally, 770 km influence radii and five-point smoothing [see *Levitus*, 1982]. This is in contrast to the XBT data which are approximately uniformly distributed in latitude along the ship transects and have only been spatially smoothed to eliminate wave numbers higher than 0.33 cycles per degree of latitude.

Deep hydrocast stations in the Levitus analysis allow consideration of various depths of no motion. Transports

relative to 400 m and 1000 m are presented here: 400 m for a comparison with XBT calculations and 1000 m for consideration of a deeper level of no motion. Below 1000 m the data are sparse, and our analyses are degraded by using reference levels deeper than 1000 m. Note that the Levitus and XBT data sets do not overlap in time and so are independent of one another.

3. DYNAMICS

Sverdrup's [1947] vertically integrated linearized vorticity and continuity equations for a Boussinesq, inviscid, incompressible, β plane ocean are used to describe the interior equatorial flow. The resulting expressions for vertically integrated meridional (V) and zonal (U) Sverdrup transports per unit width are

$$V = 1/\beta\rho_0 \operatorname{curl}_z \boldsymbol{\tau} \tag{1}$$

$$U = 1/\beta\rho_0 \int_x^0 [\partial_y \operatorname{curl}_z \boldsymbol{\tau}]\, dx \tag{2}$$

where β is the meridional gradient of the Coriolis parameter, ρ_0 is the mean water density assumed constant at 1 g cm^{-3}, $\boldsymbol{\tau}$ is the surface wind stress vector with components (τ^x, τ^y) in the x (positive east) and y (positive north) directions, $x = 0$ at the eastern basin boundary, and $U(0)$ is assumed equal to zero. Further, the stream function can be defined for horizontally nondivergent flow as $\Psi_x = V$ and $\Psi_y = -U$. Stream function fields were calculated by integrating V westward from an initial condition of $\Psi = 0$ at the eastern basin boundary.

Vertically integrated pressure P was also calculated according to

$$P = -\int_x^0 [f/\beta \operatorname{curl}_z \boldsymbol{\tau} + \tau^x]\, dx + P(0) \tag{3}$$

The boundary conditions $P(0)$ along the eastern coastline are determined by requiring no flow into the boundary, and then integrating $\partial_i P = \tau^i$, where i is the component parallel to the coast. The integration constant (i.e., $P(0)$ at 20°S) was chosen such that the mean difference between XBT and wind-derived integrated pressures along XBT transects was zero.

Geostrophic transports per unit width (U_g, V_g) were calculated as the difference between Sverdrup transports (U, V) and Ekman transports ($U_e = \tau^y/f\rho_0$, $V_e = -\tau^x/f\rho_0$):

$$U_g = 1/\beta\rho_0 \int_x^0 [\partial_y \operatorname{curl}_z \boldsymbol{\tau}]\, dx - \tau^y/f\rho_0 \tag{4}$$

$$V_g = f/\beta\rho_0 \operatorname{curl}_z(\boldsymbol{\tau}/f) \tag{5}$$

4. MODEL RESPONSE

In our study, depth-integrated pressure and geostrophic transports determined from observations are compared with those predicted by the Sverdrup model. As background, we first present maps of the Sverdrup transport stream function for each wind product (Figure 3). FSU Sverdrup transports in Figure 3*a* are similar to those published by *Meyers* [1980] using the *Wyrtki and Meyers* [1975] ship winds from 1950–1972. Likewise, they are very similar to those shown by *McPhaden and Fine* [1988] using a 23-year mean (1961–1983) of the FSU ship wind product (assuming a drag coefficient of 1.2×10^{-3}). Finally, *Kessler and Taft* [1987] published a Sverdrup stream function map calculated using the UH winds which is essentially the same as Figure 3*b*.

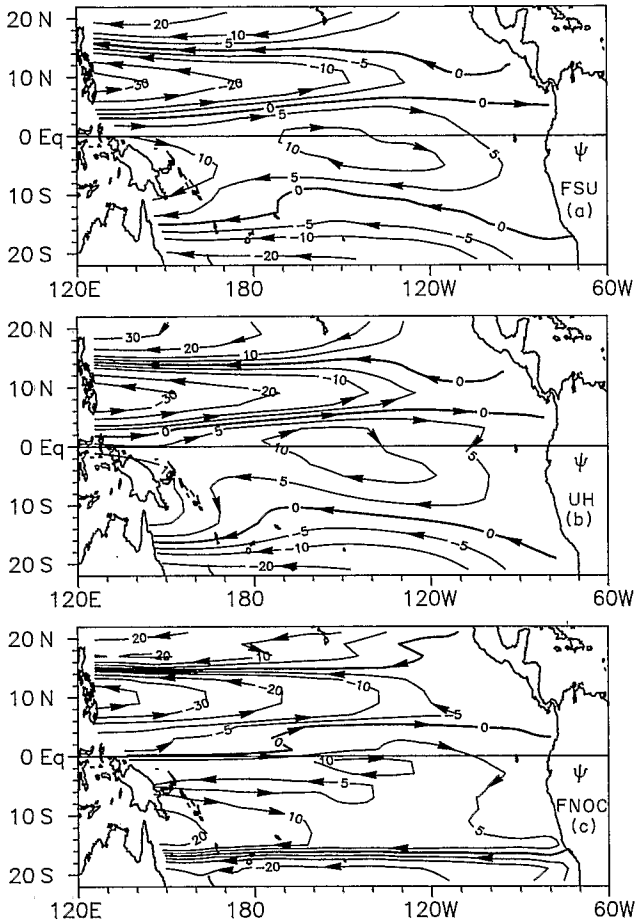

Fig. 3. Sverdrup transport stream function (in sverdrups) for (*a*) FSU, (*b*) UH, and (*c*) FNOC analyses. The contour interval is 10 Sv, with ±5 Sv also included.

All three wind products exhibit the general low latitude circulation patterns, with northern and southern subtropical and tropical gyres (Figure 3). In the northern hemisphere the westward North Equatorial Current (NEC) bifurcates at the western boundary between 14° and 16°N, as inferred from the stream function maps (i.e., where $\Psi = 0$), for all three wind products. The volume transports of the NEC range from 10 to 60 Sv (1 Sv = 10^6 m^3 s^{-1}) and those of the eastward North Equatorial Countercurrent (NECC) range from 10 to 40 Sv, with higher values to the west. A weak eastward Subtropical Countercurrent [*Yoshida and Kidokoro*, 1967] is found near 20°N, 180° in the UH calculation; it is stronger and more zonally extensive near 18°N in the FNOC calculation. In the southern hemisphere the westward South Equatorial Current (SEC) bifurcates between 15° and 17°S for all three wind products, with the volume transports ranging from 10 to 30 Sv. A weak eastward South Equatorial Countercurrent (SECC) is found in the western Pacific equatorward of about 12°S in the FSU and UH calculations; in contrast, the SECC is much stronger and

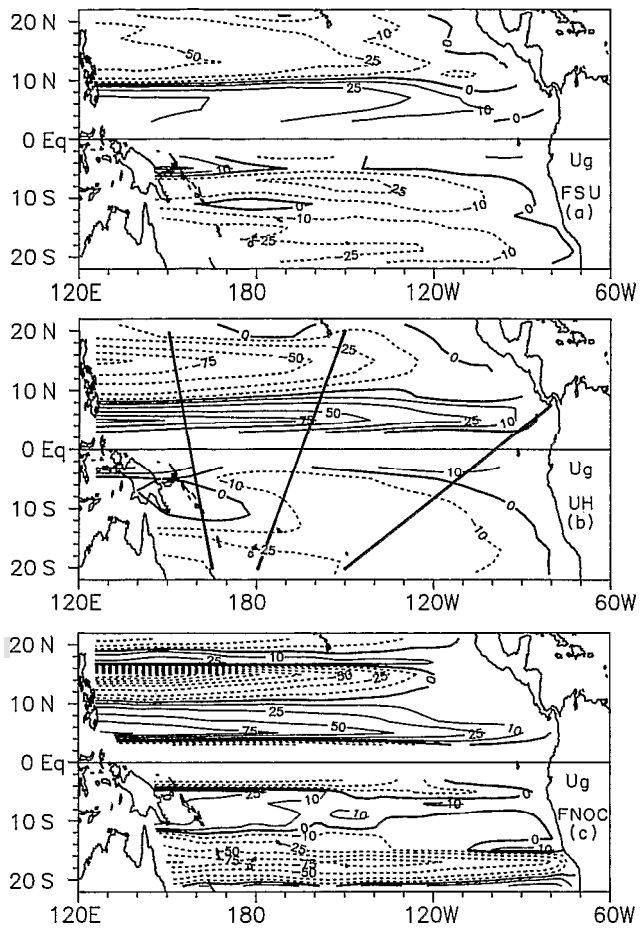

Fig. 4. Zonal geostrophic transport per unit width (in square meters per second) for (*a*) FSU, (*b*) UH, and (*c*) FNOC analyses. Solid (dashed) contours indicate eastward (westward) flow. The contour interval is 25 m^2 s^{-1}, with ±10 m^2 s^{-1} also included. XBT transect lines in the western, central, and eastern basin are indicated in Figure 4*b*.

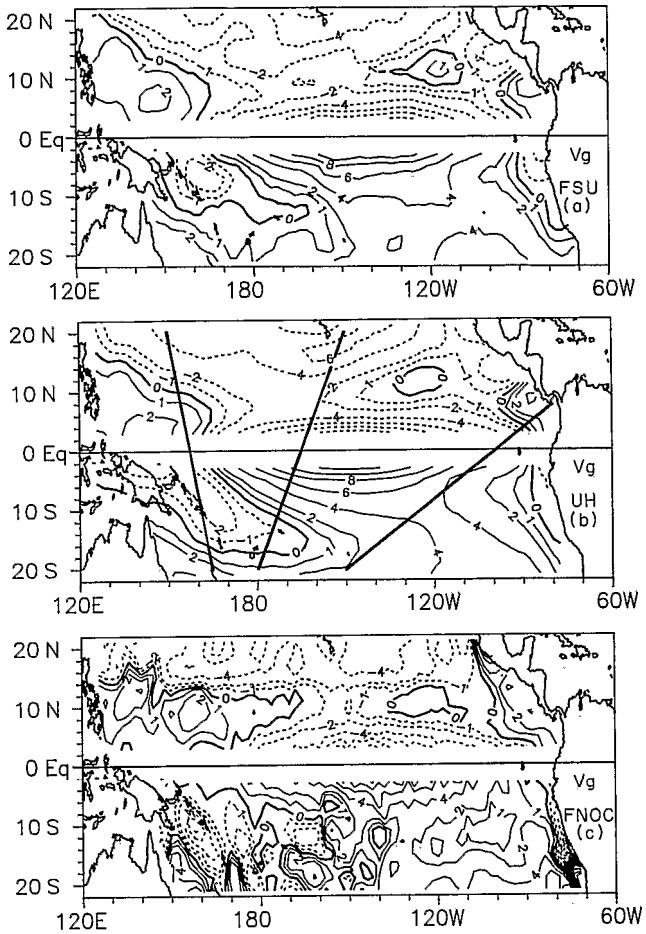

Fig. 5. Meridional geostrophic transport per unit width (in square meters per second) for (*a*) FSU, (*b*) UH, and (*c*) FNOC analyses. Solid (dashed) contours indicate northward (southward) flow. The contour interval is 2 m^2 s^{-1}, with ±1 m^2 s^{-1} also included. XBT transect lines in the western, central, and eastern basin are indicated in Figure 5*b*.

zonally extensive in the FNOC simulation because of the more zonally oriented southeast trades.

Western boundary currents (and their maximum transports between 20°N and 20°S) can be inferred from these maps: the northward flowing Kuroshio north of about 16°N (20–30 Sv), the southward flowing Mindanao between about 15°N and 2°–4°N (30–40 Sv), the northward flowing western boundary current off the New Guinea coast equatorward of about 15°S (10–20 Sv), and the southward East Australian Current poleward of 15°S (20 Sv). The boundary current off New Guinea in the FNOC calculation is qualitatively different from the FSU and UH calculations. It is twice as strong, shifted southward, and broken by a band of poleward flow near 5°S, and it does not cross the equator. Note that in order to infer these volume transports, we assumed no loss of mass through the Indonesian archipelagos although exchange through this region has been estimated to range between 1 and 9 Sv [*Gordon*, 1986].

Figures 4 and 5 show the geostrophic transport per unit width (against which XBT and Levitus data calculations will be compared) in the zonal and meridional directions, respectively. Our method of calculating transport has singularities at the equator (as $f \to 0$, U_e and $V_e \to \infty$); therefore, the region equatorward of 3° is not included in our calculation. We note that the zonal Sverdrup transport is primarily geostrophic, with $U_g \gg U_e \sim O(1$ Sv). Also, small-scale variability in FNOC curl forcing is less evident in the zonal versus meridional geostrophic flow because the former involves a zonal integration but the latter does not (compare equations (1) and (2)). The zonal geostrophic flow is also usually much stronger than the meridional flow; the latter is more intense and convergent near the equator in the central Pacific in response to zonal pressure gradients set up by easterly winds.

In general, the total and geostrophic transport calculations inferred from Figures 3 and 4 are broadly consistent with previously published estimates based on oceanic measurements of interior and boundary flows. For example, in the central Pacific, *Wyrtki and Kilonsky* [1984] reported geostrophic transports between 150°W and 158°W, south of 18°N, of 23 Sv and 20 Sv for the NEC and NECC, respectively, and 25–35 Sv of net westward flow between the equator and 17°S. These estimates are based on data collected during the Hawaii-to-Tahiti Shuttle Experiment (1979–1980), which overlaps in time with our study. In the western Pacific at 140°E, about 40 Sv was reported for the

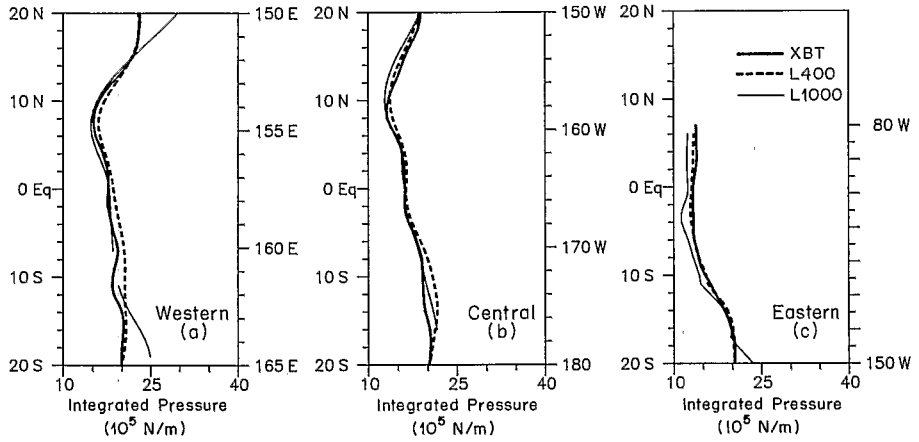

Fig. 6. Depth-integrated pressure (in units of 10^5 N m^{-1}) calculated from XBT data relative to 400 m (XBT, heavy lines), Levitus data relative to 400 m (L400, dashed lines), and Levitus data relative to 1000 m (L1000, thin lines) in the (*a*) western, (*b*) central, and (*c*) eastern Pacific.

NECC [*Wyrtki and Kendall*, 1967] and 55 Sv for the NEC [*Nitani*, 1972]. More recently, *Delcroix et al.* [1987] reported a mean value of 27 Sv for the NECC from direct current measurements along 165°E. A comparison with data along 165°E in the southern hemisphere is not as straightforward, but a mean of about 15–25 Sv net eastward transport was found poleward of 5°S. *Nitani* [1972] estimated 30 Sv of net northward transport in the Kuroshio at 20°N. *Lukas* [1988] who summarized flow estimates in the Mindanao Current, concluded that the mean transport is between 25–35 Sv. *Lindstrom et al.* [1987] found 8 Sv of northward flow through the Vitiaz Strait at 6°S, and *Church* [1987] found about 10 Sv of southward flow in the East Australian Current at 20°S. A more detailed comparison of interior geostrophic transports with transports calculated using XBT data, for the period 1979–1981, follows in section 5.2.

5. Comparison Along XBT Transects

Depth-integrated pressure and track orthogonal geostrophic transport calculations were compared along XBT transects in the western, central, and eastern basins (transects are superimposed on Figures 4*b* and 5*b*). The western and central transects run nearly north-south, and track orthogonal transports are dominated by zonal geostrophic transports. Hence when describing positive and negative track orthogonal transports in the central and western Pacific, eastward and westward will be used for convenience. In contrast, the eastern transect is more zonally oriented, and meridional transports are significant, especially near the equator, in the calculation of orthogonal track transports. Before comparing the model results with XBT data along these tracks, we first compare Levitus' historical data with the XBT data to ascertain the representativeness of the XBT data's limited 3-year coverage and 400-m maximum mean depth.

5.1. *XBT Versus Levitus Calculations*

Depth-integrated pressure and track orthogonal geostrophic transport calculated from both the augmented XBT ship of opportunity data and *Levitus* [1982] hydrographic data are presented in Figures 6 and 7, respectively. Integrated pressure calculations are very similar equatorward of 15°, especially in the northern hemisphere. The profiles define the NEC trough at 8°–10°N, a plateau within several degrees of the equator, and a rise in pressure toward the subtropical gyres poleward of 10° in both hemispheres.

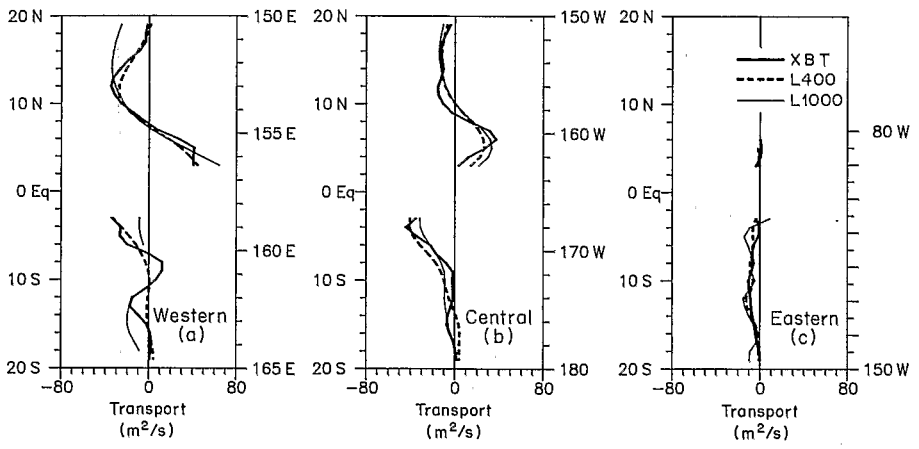

Fig. 7. Track orthogonal geostrophic transport per unit width (in square meters per second) calculated from XBT data relative to 400 m (XBT, heavy lines), Levitus data relative to 400 m (L400, dashed lines), and Levitus data relative to 1000 m (L1000, thin lines) in the (*a*) western, (*b*) central, and (*c*) eastern Pacific.

TABLE 1. Eastward Geostrophic Volume Transports Orthogonal to XBT Transects in the Latitude Band of the NECC

Data Source	Central Transect		Western Transect	
	Latitudinal Range, deg	Transport, Sv	Latitudinal Range, deg	Transport, Sv
Observations				
XBT	3–8	17	3–7	19
L400	3–10	19	3–7	16
L1000	3–10	23	3–7	20
Model				
FSU	3–10	29	3–9	33
UH	3–9	34	3–8	36
FNOC	4–10	29	4–10	40

Based on XBT data relative to 400 m (XBT), Levitus data relative to 400 m (L400), Levitus data relative to 1000 m (L1000), and Sverdrup model calculations driven by FSU, UH, and FNOC wind products.

Along the western track, pressure calculated relative to 1000 m (L1000) continues to rise poleward of 15°, whereas pressure calculated relative to 400 m (L400) using both sources levels off. Similar tendencies are observed along the eastern transect south of 18°S. This is due to the shallow reference levels of the L400 and XBT data sets relative to the depth of the main thermocline, which extends deeper than 400 m outside the equatorial region (see also *Wyrtki* [1975]; *Rebert et al.* [1985]; and *Delcroix et al.* [1987]). Along the central Pacific transect, however, the XBT, L400, and L1000 calculations are comparable in the northern hemisphere all the way to 20°N because the thermocline is sharp and confined to depths shallower than 400 m [*Kessler and Taft*, 1987].

Transport calculations (Figure 7) in the northern hemisphere equatorward of 15° depict similar boundaries between the NEC and NECC, with transports increasing from east to west. In the central Pacific, where the southern flank of the NECC is best resolved in our calculations, total volume transports are 17 Sv, 19 Sv, and 23 Sv for XBT, L400, and L1000, respectively (Table 1). These are comparable to historical calculations at 165°W of 18–20 Sv by *Wyrtki and Kendall* [1967] and *Wyrtki and Kilonsky* [1984]. Eastward transports along the western transect north of 3°N are 19 Sv, 16 Sv, and 20 Sv for XBT, L400, and L1000, respectively. Note that these transports along the western transect may underestimate flow in the NECC, since its southern boundary is not resolved in our calculations. Transport calculations from Levitus and XBT data in the southern hemisphere are also similar, except in the western basin where the Levitus data are too sparse and too heavily smoothed to define alternating SEC and SECC flow structures.

Difference plots of Levitus less XBT data are presented in Figure 8. Estimated standard error envelopes were calculated assuming that the mean surface dynamic heights calculated from each data set are subject to a 1 dyn cm error and that this error linearly decreases to zero at 400 m. It was also assumed that the errors are uncorrelated over 1° of latitude (the resolution at which the XBT and Levitus data are available). These error estimates decrease from west to east because the along-track distance for 1° latitudinal resolution increases from west to east owing to the orientations of the tracks. Differences between Levitus and XBT calculations equatorward of 15° are generally not larger than the assumed sampling error of the two data sets. Furthermore, L400 and XBT are very similar at higher latitudes. Thus these results suggest that in general, the 3-year mean derived from XBT data is representative of the long-term mean based on historical data and that a 400-m mean maximum depth is not a limiting factor equatorward of 15°.

5.2. *Model Results Versus XBT Calculations*

Depth-integrated pressures in the western, central, and eastern Pacific derived from Sverdrup dynamics are compared to XBT-based estimates (Figure 9). All model pressure calculations, as with the XBT calculation, show a NECC trough between 8° and 10°N and a relatively flat topography within several degrees of the equator. Deviations from observations generally increase toward the west and are largest for the FNOC model response. The FNOC response also shows a very well defined SECC trough centered near 14°S that is not present in the XBT data. Poleward of 15° the NEC and SEC ridges of the wind products also appear exaggerated compared with those of the XBT as expected

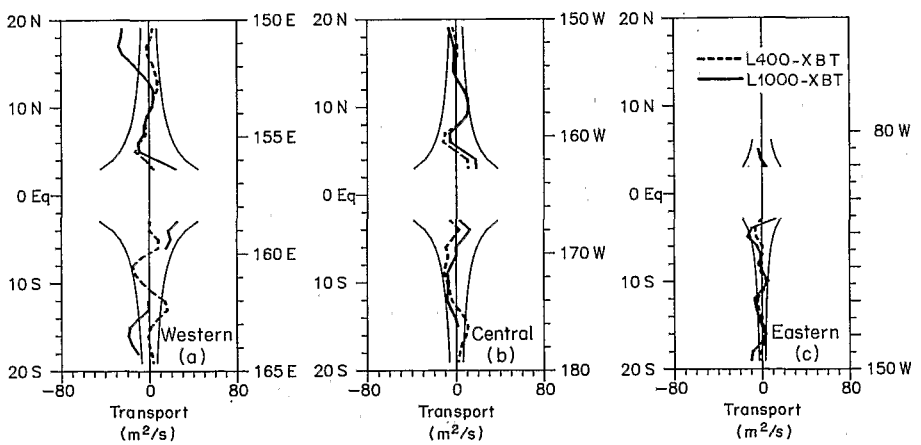

Fig. 8. Differences between track orthogonal geostrophic transport per unit width (in square meters per second) in the (*a*) western, (*b*) central, and (*c*) eastern Pacific. Solid and dashed lines are for L1000-XBT and L400-XBT, respectively. Smooth curves are standard error envelopes assuming a 1 dyn cm error in surface dynamic height, linearly decreasing to zero at 400 m for both Levitus and XBT data (see text for discussion).

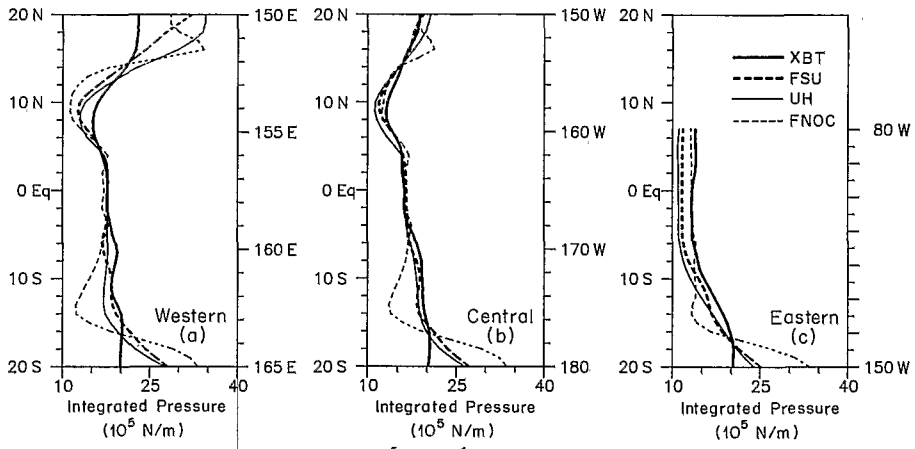

Fig. 9. Depth-integrated pressure (in units of 10^5 N m^{-1}) calculated from XBT data relative to 400 m (heavy lines) and Sverdrup dynamics forced by FSU winds (thick dashed lines), UH winds (thin lines), and FNOC winds (thin dashed lines) in the (*a*) western, (*b*) central, and (*c*) eastern Pacific.

from the comparison of L1000 with L400 and XBT (Figure 6). However, in general, the structures of FSU and UH are comparable to L1000 in these regions, whereas the NEC and SEC ridges of FNOC are larger.

Track orthogonal transports calculated from the Sverdrup model and from the XBT data are shown in Figure 10. All three wind products describe the general structure of the NEC and NECC. However, model transports are larger in the NEC and NECC compared to XBT (or Levitus) transports, with deviations from the XBT calculations increasing to the west. For example, in the central Pacific, where the southern flank of the NECC is best resolved, volume transports in the NECC are computed to be 29 Sv (FSU), 34 Sv (UH), and 39 Sv (FNOC), compared with 17–23 Sv calculated from XBT and Levitus data; in the western Pacific, eastward transports north of 3°N are 33 Sv (FSU), 36 Sv (UH), and 40 Sv (FNOC), compared with 16–19 Sv calculated from in situ data (Table 1).

In the southern hemisphere, FSU, UH, and XBT transports are qualitatively similar in the eastern and central basin. Along the western track between 3°S and 10°S, however, there is no consistent correspondence in sign or magnitude of the XBT, FSU, UH, or FNOC results, although the XBT calculation defines strong westward flow equatorward of 6°S, whereas the three wind products describe eastward or weak westward flow. Also, poleward of 15°S on all the transects, the model responses describe stronger westward transport than observed in the XBT data (or the L1000 calculation in Figure 7).

The differences between modeled and observed transports are shown in Figure 11. Standard error envelopes comparable to those in Figure 8 are also plotted assuming a 1 dyn cm error in mean XBT dynamic heights; these envelopes are smaller by a factor of $2^{1/2}$ since no attempt was made to evaluate the error in the Sverdrup model response. We note that the differences in Figure 11 are much larger than the differences between Levitus data and XBT data (Figure 8) and more often than not exceed our crude estimate of uncertainty in XBT-derived transports.

Table 2 quantifies differences between 15°N to 15°S using an estimate of the signal-to-noise ratio given by $r = \sigma_{XBT}/\sigma_{XBT\text{-}model}$. We note that the ratios for the FSU and UH model responses are equal along each track and $r > 1$, where $r < 1$ for the FNOC response. Also, in general r decreases to the west consistent with the fact that the differences in Figure 11 increase toward the west. For comparison, Table

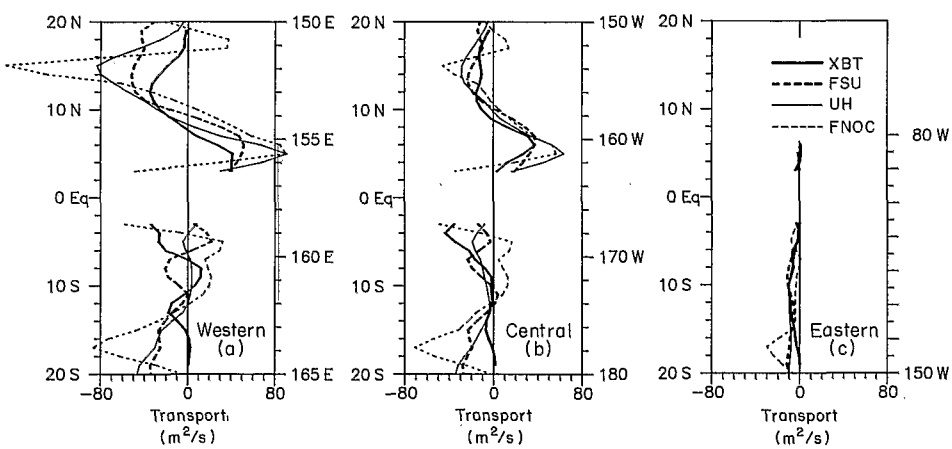

Fig. 10. Track orthogonal geostrophic transport per unit width (in square meters per second) calculated from XBT data relative to 400 m (heavy lines) and Sverdrup dynamics forced by FSU winds (thick dashed lines), UH winds (thin lines), and FNOC winds (thin dashed lines) in the (*a*) western, (*b*) central, and (*c*) eastern Pacific.

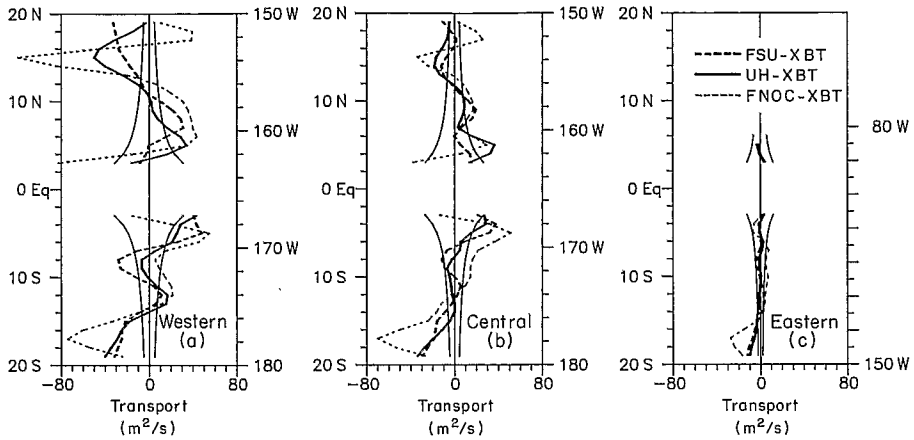

Fig. 11. Differences between track orthogonal geostrophic transport per unit width (in square meters per second) in the (*a*) western, (*b*) central, and (*c*) eastern Pacific. Thick dashed lines are for FSU-XBT, solid lines are for UH-XBT, and thin dashed lines are for FNOC-XBT. Smooth curves are error envelopes assuming a 1 dyn cm error in surface dynamic height, linearly decreasing to zero at 400 m for the XBT data (see text for discussion).

2 also shows the signal-to-noise ratios for XBT and Levitus transports, $r = \sigma_{XBT}/\sigma_{XBT\text{-}Levitus}$. These are typically larger than unity and, in contrast to the XBT-model calculations, largest in the west. With the exception of the eastern Pacific where signal amplitudes are small, the signal-to-noise ratio for the XBT-model comparison is smaller than the signal-to-noise ratio for the XBT-Levitus comparison.

6. Summary and Discussion

Differences between XBT transports and Sverdrup model transports are both quantitative (e.g., 50–100% relative errors in NECC magnitudes) and qualitative (e.g., oppositely directed currents in the southern hemisphere). Differences between the XBT and Levitus transports are generally significantly smaller (compare Figures 8 and 11; and Tables 1 and 2). This suggests that (1) Sverdrup dynamics does not apply and/or (2) there are inaccuracies in the mean wind stresses that contaminate the Sverdrup solutions. We discuss each of these possibilities in turn.

Sverdrup theory assumes that the ocean is in steady equilibrium with the winds. In support of this, we have shown that equatorward of 15° depth-integrated geostrophic transports calculated with the 3-year average of the 1979–1981 XBT data relative to 400 m are comparable to transports calculated using the long-term Levitus mean data relative to 400 m and 1000 m. *Philander* [1979] argues that the tropical ocean equatorward of about 15° should adjust to idealized transient forcing on a 3- to 5-year time scale based on the group speeds of long Rossby waves. However, in numerical general circulation model studies with observed winds, the adjustment time for the upper few hundred meters of the tropical Pacific was found to be closer to 2 years [e.g., *Philander et al.*, 1987]. Hence differences between the observations and the Sverdrup model due to ocean transients should be small.

Sverdrup theory neglects nonlinearity, which could be important for transports in the Equatorial Undercurrent [*Philander and Pacanowski*, 1980; *McPhaden and Taft*, 1988]. However, latitudes equatorward of 3° have been excluded from our transport analysis. *Spillane and Niiler* [1975] suggested that nonlinearity is important in the NECC and that it would lead to a stronger and narrower current than predicted by Sverdrup theory. In the central Pacific where our calculations resolve the southern boundary of the NECC, it is arguable that the NECC is narrower relative to the Sverdrup calculations (e.g., Figure 7); however, the observed NECC transports are clearly not stronger (Table 1). This is also evident in the western Pacific, where the modeled transports are stronger (or comparable) than our (or historical) transports calculated from Levitus or XBT data. Further, previously published transports are comparable or less [e.g., *Wyrtki and Kendall*, 1967; *Delcroix et al.*, 1987], none appear to be stronger than the model calculations. Thus it is not obvious to us that nonlinearity can explain the differences between observed and modeled transports in the NECC or elsewhere.

It is possible that lateral friction might be important in the NECC. However, *McPhaden et al.* [1988] found for a linear multi-vertical mode model (whose steady solution is governed by Sverdrup dynamics) that results were insensitive to variations in lateral diffusion over a range of 1×10^7 cm^2 s^{-1} to 5×10^7 cm^2 s^{-1}. It is unlikely that larger values of diffusivity can be justified in the tropics. Thus we conclude that deviations from Sverdrup dynamics, if they exist, are not the limiting factor in our comparisons with the observations.

TABLE 2. Estimate of the Signal-to-Noise Ratio

	Western	Central	Eastern
Model			
FSU	1.1	1.3	1.6
UH	1.1	1.3	1.6
FNOC	0.6	0.8	0.8
Observations			
L400	2.9	2.4	1.2
L1000	1.9	2.3	0.6

The signal-to-noise ratio is calculated as $r = \sigma_{XBT}/\sigma_{Dif}$, where σ_{XBT} is the standard deviation of track orthogonal geostrophic transport between 15°N and 15°S (excluding 3°N to 3°S) based on XBT data and σ_{Dif} is the standard deviation of the difference between XBT-derived transports and those derived from the Sverdrup dynamics or Levitus data.

Uncertainties in the magnitude of a constant drag coefficient can account for only 10–20% of the quantitative differences and none of the qualitative differences between observed and modeled transports. Allowing the drag coefficient to vary [e.g., *Saunders*, 1976] should not introduce significant qualitative changes in the Sverdrup calculation. Hence inaccuracies in the wind stress products are probably responsible for the major discrepancies between the observations and model. This would explain why the differences between the FSU, UH, and FNOC-derived model results are sometimes as large as differences between individual model results and the observations. The fact that the largest discrepancies are found along the western track is consistent with an accumulation of error towards the west from zonal integration of the solution (e.g., equation (2)).

In conclusion, we have shown that estimates of Sverdrup transport in the tropical Pacific are sensitive to the choice of wind stress forcing. This implies that accurate and detailed simulation of the general circulation will require better wind estimates than are currently available. Errors in wind stress forcing affect not only the interior ocean but the western boundary as well, since systematic errors in the wind field accumulate toward the west. This could lead to considerable uncertainty in model studies of higher-order processes such as meridional heat transport, which depend on accurate simulation of both interior and western boundary currents. It is interesting to note that the subjective analyses (FSU and UH) compare more favorably with the observations than does the objective FNOC analysis. All three products rely heavily on ship wind reports; the UH and FNOC analyses incorporate satellite cloud motion vector, island, and buoy winds. Thus it is clear that analysis procedures are as important as data sources and data availability in determining the quality of a wind product.

Acknowledgments. Portions of this work were in partial fulfilment of M.C.L.'s Master of Science degree at the University of Washington under the guidance of M.J.M. We would like to thank the members of her advisory committee, Bruce Taft, Lewis Rothstein, and Paul Quay, for their encouragement. We would also like to thank Gary Raymond for his programming assistance. The FSU wind product was provided by James J. O'Brien, the UH product by James Sadler, and the FNOC product by John Kindle. This work was supported by NOAA's Equatorial Pacific Ocean Climate Studies (EPOCS) program (M.J.M. and M.C.L.), School of Oceanography, UW (M.C.L.), and ORSTOM through a PNEDC contract (J.P.). School of Oceanography, UW, contribution 1821; Joint Institute for Study of the Atmosphere and Ocean, UW, contribution 62; NOAA Pacific Marine Environmental Laboratory contribution 1045.

REFERENCES

Cane, M. A., S. E. Zebiak, and S. C. Dolan, Experimental forecasts of El Niño, *Nature*, *321*, 827–832, 1986.

Church, J. A., East Australian Current adjacent to the Great Barrier Reef, *Aust. J. Mar. Freshwater Res.*, *38*, 671–683, 1987.

Cressman, G. P., An operational objective analysis system, *Mon. Weather Rev.*, *87*, 367–374, 1959.

Delcroix, T., G. Eldin, and C. Hénin, Upper ocean water masses and transports in the western tropical Pacific (165°E), *J. Phys. Oceanogr.*, *17*, 2248–2262, 1987.

Evenson, A. J., and G. Veronis, Continuous representation of wind stress and wind stress curl over the world ocean, *J. Mar. Res.*, *33*, suppl., 131–144, 1975.

Godfrey, J. S., A Sverdrup model of the depth-integrated flow for the world ocean allowing for island circulations, *J. Mar. Res.*, in press, 1989.

Goldenberg, S. B., and J. J. O'Brien, Time and space variability of tropical Pacific wind stress, *Mon. Weather Rev.*, *109*, 1190–1207, 1981.

Gordon, A. L., Interocean exchange of thermocline water, *J. Geophys. Res.*, *91*, 5037–5046, 1986.

Halpern, D., and D. E. Harrison, Intercomparison of tropical Pacific mean November 1979 surface wind fields, *Tech. Rep. 82-1*, 40 pp., Dep. of Meteorol. and Phys. Oceanogr., Mass. Inst. of Technol., Cambridge, 1982.

Harrison, D. E., W. S. Kessler, and B. S. Geise, Ocean circulation model hindcasts of the 1982–83 El Niño thermal variability along ship-of-opportunity tracks, *J. Phys. Oceanogr.*, *19*, 397–418, 1989.

Kessler, W. S., and B. A. Taft, Dynamic heights and zonal geostrophic transports in the central tropical Pacific during 1979–1984, *J. Phys. Oceanogr.*, *17*, 97–122, 1987.

Large, W. G., and S. Pond, Open ocean momentum flux measurements in moderate to strong winds, *J. Phys. Oceanogr.*, *11*, 324–336, 1981.

Leetmaa, A., P. Niiler, and H. Stommel, Does the Sverdrup relation account for the mid-Atlantic circulation?, *J. Mar. Res.*, *35*, 1–10, 1977.

Levitus, S., Climatological atlas of the world ocean, *NOAA Prof. Pap. 13*, 173 pp., U. S. Government Printing Office, Washington, D. C., 1982.

Lindstrom, E., R. Lukas, R. Fine, E. Firing, S. Godfrey, G. Meyers, and M. Tsuchiya, The Western Equatorial Pacific Ocean Circulation Study, *Nature*, *330*, 533–537, 1987.

Lukas, R., Interannual fluctuations of the Mindanao Current inferred from sea level, *J. Geophys. Res.*, *93*, 6744–6748, 1988.

McPhaden, M. J., and R. A. Fine, A dynamical interpretation for the tritium maximum in the central equatorial Pacific, *J. Phys. Oceanogr.*, *18*, 1454–1457, 1988.

McPhaden, M. J., and B. A. Taft, On the dynamics of seasonal and intra-seasonal variability in the eastern equatorial Pacific, *J. Phys. Oceanogr.*, *18*, 1713–1732, 1988.

McPhaden, M. J., A. J. Busalacchi, and J. Picaut, Observations of wind-forced model simulations of the mean seasonal cycle in tropical Pacific sea surface topography, *J. Geophys. Res.*, *93*, 8131–8146, 1988.

Meyers, G., Do Sverdrup transports account for the Pacific North Equatorial Countercurrent?, *J. Geophys. Res.*, *85*, 1073–1075, 1980.

Meyers, G., and J. R. Donguy, An XBT network with merchant ships, *Tropical Ocean-Atmos. Newsl. 2*, pp. 6–7, Equatorial Pac. Ocean Clim. Stud., Natl. Oceanic and Atmos. Admin., 1980.

Mitchum, G. T., A bias in the satellite-observed low-level cloud motion winds over the central tropical Pacific, *J. Geophys. Res.*, *92*, 3861–3866, 1987.

Nitani, H., Beginning of the Kuroshio, in *Kuroshio: Physical Aspects of the Japan Current*, edited by H. Stommel and K. Yoshida, pp. 129–163, University of Washington Press, Seattle, 1972.

Philander, S. G. H., Variability of the tropical oceans, *Dyn. Atmos. Oceans*, *3*, 191–208, 1979.

Philander, S. G. H., and R. C. Pacanowski, The generation of equatorial currents, *J. Geophys. Res.*, *85*, 1123–1136, 1980.

Philander, S. G. H., W. J. Hurlin, and A. D. Seigel, Simulation of the seasonal cycle of the tropical Pacific Ocean, *J. Phys. Oceanogr.*, *17*, 1986–2002, 1987.

Rebert, J.-P., J. R. Donguy, G. Eldin, and K. Wyrtki, Relations between sea level, thermocline depth, heat content, and dynamic height in the tropical Pacific Ocean, *J. Geophys. Res.*, *90*, 11,719–11,725, 1985.

Sadler, J. C., and B. J. Kilonsky, Deriving surface winds from satellite observations of low-level cloud motions, *J. Clim. Appl. Meteorol.*, *24*, 758–769, 1985.

Sadler, J. C., M. A. Lander, A. M. Hori, and L. K. Oda, Tropical marine climatic atlas, vol. II, Pacific Ocean, *Tech. Rep. UHMET 87-02*, Dep. of Meteorol., Univ. of Hawaii, Honolulu, 1987.

Saunders, P. M., On the uncertainty of wind stress curl calculations, *J. Mar. Res.*, *34*, 155–160, 1976.

Schopf, P. S., and M. J. Suarez, Vacillations in a coupled ocean-atmosphere model, *J. Atmos. Sci.*, *45*, 549–566, 1988.

Spillane, M., and P. P. Niiler, On the theory of strong, midlatitude wind-driven ocean circulation, I, The North Pacific Countercur-

rent as a quasi-geostrophic jet, *Geophys. Fluid Dyn.*, *7*, 43–66, 1975.

Sverdrup, H. U., Wind-driven currents in a baroclinic ocean, with application to the equatorial currents of the eastern Pacific, *Proc. Natl. Acad. Sci. U.S.*, *33*, 318–326, 1947.

Welander, P., On the vertically integrated mass transport in the oceans, in *The Atmosphere and Sea in Motion: Scientific Contributions to the Rossby Memorial Volume*, edited by B. Bolin, pp. 95–101, The Rockefeller Institute Press, New York, 1959.

White, W. B., G. Meyers, and K. Hasunuma, Space/time statistics of short-term climatic variability in the western north Pacific, *J. Geophys. Res.*, *87*, 1979–1989, 1982.

Wyrtki, K., Fluctuations of the dynamic topography in the Pacific Ocean, *J. Phys. Oceanogr.*, *5*, 450–459, 1975.

Wyrtki, K., and R. Kendall, Transports of the Pacific Equatorial Countercurrent, *J. Geophys. Res.*, *72*, 2073–2076, 1967.

Wyrtki, K., and B. Kilonsky, Mean water and current structure during the Hawaii-to-Tahiti Shuttle Experiment, *J. Phys. Oceanogr.*, *14*, 242–254, 1984.

Wyrtki, K., and G. Meyers, The trade wind field over the Pacific Ocean, I, The mean field and the mean annual variation, *Tech. Rep. HIG-75-1*, 26 pp., Hawaii Inst. of Geophys., Honolulu, 1975.

Yoshida, K., and T. Kidokoro, A subtropical countercurrent, II, A prediction of eastward flows at lower subtropical latitudes, *J. Oceanogr. Soc. Jpn.*, *23*, 231–246, 1967.

Zebiak, S. E., and M. A. Cane, A model of El Niño–Southern Oscillation, *Mon. Weather Rev.*, *115*, 2262–2278, 1987.

M. C. Landsteiner, School of Oceanography, WB-10, University of Washington, Seattle, WA 98195.

M. J. McPhaden, NOAA Pacific Marine Environmental Laboratory, Seattle, WA 98115.

J. Picaut, Groupe SURTROPAC, ORSTOM, Nouméa, New Caledonia.

(Received September 23, 1988;
accepted June 29, 1989.)